Application of Secondary Nucleation Theory to Semirigid Macromolecules: PEEK, PET, and PEN

F. J. Medellín-Rodríguez and P. J. Phillips*

Department of Materials Science and Engineering, The University of Tennessee, Knoxville, Tennessee 37996-2000

J. S. Lin

Solid State Division, Oak Ridge National Laboratory, Oak Ridge, Tennessee 37831

Received January 23, 1995; Revised Manuscript Received August 28, 1995[⊗]

ABSTRACT: A study of the applicability of secondary nucleation theory to the semirigid macromolecules poly(aryl ether ether ketone) (PEEK), poly(ethylene terephthalate) (PET), and poly(ethylene naphthalenate) (PEN) has been made. The main purpose of the study was to test the latest version of secondary nucleation theory, which permits the estimation of the lateral surface free energy from the characteristic ratio, C_∞. This was made through a numerical comparison of theoretical and experimental values of the products of the lateral and fold surface free energies $\sigma\sigma_e$. The surface free energy products were obtained from the direct application of the latest version of secondary nucleation theory to experimental data and compared to calculated values. Computation of the C_∞ values was made assuming that these macromolecules can be considered as polymeric chains with virtual bonds. Direct evaluations of the fold surface free energy σ_e used the well-known expression derived from secondary nucleation theory for the lamellar thickness as a function of supercooling. Other evaluations of σ and σ_e were also made where possible, and they ranged from fundamental (Thomson−Gibbs) to empirical (Thomas−Stavely/Kaelble−Cirlin) methods. The product of surface free energies obtained from analysis of the experimental growth rates was always higher than the calculated values by a significant factor. Better numerical agreement was obtained if the data were analyzed assuming that only regime III was present. However, overall, it was concluded that the latest version of secondary nucleation theory does not quantitatively account for the crystallization behavior of this group of semirigid macromolecules.

Introduction

Application of mathematical or numerical models to explain the crystallization behavior of semicrystalline polymers has been the topic of two main groups of scientific papers.[1−12] Secondary nucleation theory for polymers was developed originally using a realistic molecular model by Hoffman, Lauritzen, *et al.*[1−8] and is considered by many to be satisfactory in explaining the crystallization behavior of macromolecules such as polyethylene[2] and other relatively flexible polymers.[8] The most recent novel attempt to explain the crystallization process of macromolecules was the surface-roughening model developed by Sadler *et al.*[9−12] It was based on crystallization concepts known to apply to metals, together with relatively unsophisticated computer simulations. However, years before, secondary nucleation theory provided a kinetic model with broader mathematical arguments and much clearer molecular explanations, which made it successful through the years.

As first proposed, secondary nucleation theory assumes that crystal growth is a continuous process of nucleation of molecular segments onto an existing primary crystalline nucleus. In one of the broadest expositions of the model,[2] it is considered that a portion of the chain adsorbs first on the primary nucleus and then the rest of the macromolecule spreads laterally in an adjacently reentered manner, giving rise to a monolayer. In the latest, more refined version,[7,8] a much clearer molecular explanation is given for the valid form of the model, the so-called "low-Ψ" form. This involves random attachment of segments from unperturbed conformations onto a primary nucleus, reorganization on the surface, and finally crystallographic register. This last "negentropic" explanation also generated, for the first time, a theory which incorporates one of the most important characteristic parameters of the individual molecule, namely the characteristic ratio, C_∞. Indeed the method of introduction of the parameter, through a change of energy, generated a mathematical expression for one of the least understood parameters in crystallization of polymers, the lateral surface free energy σ. The computation of the value of C_∞ for each polymer under consideration therefore becomes an important matter in interpretation of crystallization behavior and requires either the direct use of statistical mechanics or the application of a simplified statistical model appropriate for the particular macromolecule.

Prior to this most recent development, the most significant advance was the introduction of regimes in which competition between the rate of deposition of critical nuclei and the rate of surface spreading generate three different regimes of growth (see refs 13 and 14 for a review). In practice, the process of surface spreading on the growth face involves two competitive processes. These are (a) adjacent reentry by a contiguous section of the molecule which formed the critical nucleus and (b) the deposition of a nonadjacent section of the same molecule or of a section of a different molecule in the adjacent position.

In its most successful form, secondary nucleation theory for polymers explains adequately, in both qualitative and quantitative forms, the behavior of a flexible polymer such as linear polyethylene, where the surface spreading process occurs most effectively if adjacent reentry of molecules is assumed. This occurs largely because the reptation process is sufficiently fast to permit adjacent reentry to occur at a rate consistent

* To whom correspondence should be sent.

[⊗] Abstract published in *Advance ACS Abstracts,* October 15, 1995.

0024-9297/95/2228-7744$09.00/0

with the energetics of the process. For less flexible molecules, particularly if they have aromatic backbones, two molecular constraints occur which may prevent the adjacent reentry process from prevailing over the competing process of deposition of part of another molecule (or of the same molecule) in the adjacent position.

First, lower flexibility results in a low rate of reptation and will make the deposition of a second molecule in the adjacent position more likely. Second, and more impressively when it occurs, the geometrical constraints of the chain may make adjacent reentry physically impossible. In both cases, the interface between the crystal and the amorphous phase becomes macroscopic and it becomes essentially a third phase, rendering the underlying thermodynamic basis of secondary nucleation theory problematic.

A series of polymers of decreasing flexibility, due to aromaticity in the backbone, are poly(ethylene terephthalate) (PET), poly(ethylene naphthalenate) (PEN), and poly(ether ether ketone) (PEEK). Earlier versions of secondary nucleation theory have already been used in a limited range of temperatures with PEEK[15,16] and also with PET;[17,18] however, it has not been applied to PEN. On the other hand, an analysis comparing flexible macromolecules with a family of polymers with potentially different crystallization behavior, because of the inherent rigidity of the chains, has not yet been made.

This study reports the attempted application of the most recent version of secondary nucleation theory to the crystallization behavior of PEEK, PEN, and PET. Values of the lateral surface free energy σ and of the fold surface free energy σ_e have been obtained theoretically or from lamellar thickness studies. This was done in order to compare such values with the products $\sigma\sigma_e$ that emerge from the direct application of the theory to linear growth data. The selected polymers exhibit a wide range of crystallization features such as changes in morphology, changes in crystalline structure, and changes in growth rates as a function of the degree of supercooling. Additionally, however, because of their stiffness, they will exhibit relatively high values of C_∞ resulting in relatively low values of σ, providing an extreme test of the applicability of the most advanced form of secondary nucleation theory currently available.

Theoretical Approaches

The main requirements of the regimes version of secondary nucleation theory (SNT)[8] are physical adsorption of short molecular segments onto a crystal nucleus (secondary nucleation), lateral migration of such segments on the surface of the nucleus, and finally crystallographic register. It is also considered that the macromolecule adopts unperturbed dimensions in the molten state before crystallizing and that as soon as it is "localized", it loses entropy. Therefore, two physical states are the point of departure in the theory, literally[8] (1) the isotropic molten state with unperturbed dimensions and (2) a "localized" activated complex similar to physical adsorption. The incremental change of free energy to pass from state 1 to state 2 is given by[7]

$$\Delta G^*_{1\to 2} = \frac{T\Delta h_f a_0 b_0 l_u n^*}{T_m^\circ}\frac{1}{C_\infty} \qquad (1)$$

where Δh_f is the latent heat of fusion, a_0 and b_0 are the lattice parameters characterizing the chain cross-section, l_u is the mer length, and n^* is the number of mers in a stem.

Table 1. Unit Cell Type, Molecular Width a_0, and Monomolecular Layer Thickness b_0 of PET, PEN, and PEEK

polymer	unit cell type	a_0, b_0 (Å)
PET	triclinic	4.56, 5.50
PEN	triclinic, α	6.51, 5.60
PEEK	orthorhombic	4.86, 4.60

After applying a free energy balance on the crystalline surface,[7] the cost in free energy of crystallization of the first segment is given by

$$\Delta G^*_{1\to 2} = 2b_0\sigma l_u n^* - \Psi a_0 b_0 l_u n^*(\Delta G_c') \qquad (2)$$

The mathematically valid form of the SNT model involves $\Psi = 0$. Therefore, after comparing eqs 1 and 2 for the case of semirigid macromolecules, the lateral surface free energy, assuming T is approximately equal to T_m, is given by

$$\sigma_{theor} = \Delta h_f(a_0/2)(1/C_\infty) \qquad (3)$$

In eq 3, the parameter C_∞ is the characteristic ratio and it is related to the unperturbed dimensions of the macromolecule.[19-21]

Determination of the cross-sectional area of the macromolecules once they crystallize is made in accordance with the Bravais–Friedel law. In accordance with this law, crystalline planes with the largest spacing will be preferred for growth. Geometrical and symmetrical considerations of each unit cell are utilized in the estimation of the largest spacing. In this form, the monomolecular layer thickness b_0 and the molecular width a_0 are numerically obtained as shown in Table 1.

C_∞ is the infinite molecular weight value of the characteristic ratio C_n. The characteristic ratio takes into account short-range interactions and can be defined as the ratio of the average root mean square end-to-end distance of the unperturbed chain in the absence of long-range interactions to the average root mean square end-to-end distance of a random-flight chain.[19-21]

$$\frac{\langle \bar{r}^2\rangle_0^{1/2}}{\langle \bar{r}^2\rangle_{fj}^{1/2}} = \frac{C_n l x^{1/2}}{l x^{1/2}} \qquad (4)$$

Since $\langle \bar{r}^2\rangle_{fj}^{1/2}/lx^{1/2} = 1$, then

$$C_n = \frac{\langle \bar{r}^2\rangle_0^{1/2}}{l x^{1/2}} \qquad (5)$$

The theoretical estimation of C_∞ was one of the main problems in this study. On the basis of statistical mechanics, Flory[20] completed rigorous calculations of C_∞ for a number of macromolecules. However, after surveying the literature, of the three polymers in this study, theoretical data were found only for PET.[22] Therefore, determination of C_∞ for PEEK and PEN required first the calculation of the average square end-to-end distance of the macromolecules with unperturbed dimensions.

A relatively simple model proposed by Benoit,[23] which assumes chains with free rotation of virtual bonds and no molecular interactions, was used in this work in order to estimate the mean square end-to-end distance $\langle r^2\rangle_0$. A "calibration" procedure was made and it followed several steps. First, PET was taken as a "standard" and two C_∞ theoretical values emerging from two different configurations, as determined by Williams and

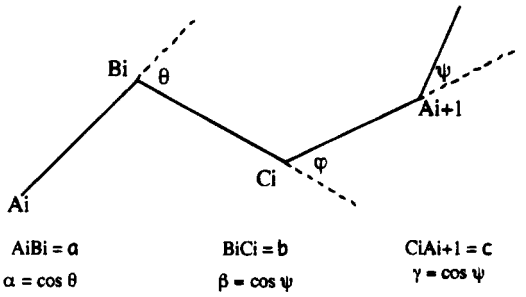

Figure 1. General representation of monomeric units with virtual bonds (after Benoit, 1948).

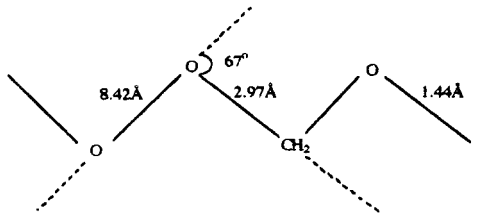

Figure 2. Monomeric unit of PET with three virtual bonds.

Table 2. End-to-End Distances of PET Evaluated by Two Different Methods

method	no. of bonds	$\langle r^2\rangle_0$ (Å)
Williams, Flory	6 (1 virtual)	19 653
Williams, Flory	4 (2 virtual)	34 167
Benoit	3 (3 virtual)	20 740

Flory,[22] were taken as the reference. Second, the mean square end-to-end distance of PET was calculated using Benoit's model[23] for two polymeric chains with different numbers of total and virtual bonds: (i) considering 6 bonds along the monomeric unit (1 virtual) and (ii) considering 4 bonds (2 virtual). Calculations were made considering n_z, the number of skeletal bonds along the chain and assuming also a most probable molecular weight distribution ($\bar{M}_n$:$\bar{M}_w$:$\bar{M}_z$ = 1:2:3). This last assumption was made considering the type of synthesis involved (polycondensation) for all three polymers. Benoit's equation for peptidic chains[23] as given by eq 6 was applied to obtain the desired values

$$\langle r^2\rangle_0 = \frac{p}{1-\alpha\beta\gamma}\{(a^2+b^2+c^2)+2(ab\alpha+bc\beta+ca\gamma)+2ab\beta\gamma+2bc\gamma\alpha+2ca\alpha\beta\}+2\frac{\alpha\beta\gamma^p-1}{1-\alpha\beta\gamma}\{\alpha\beta\gamma(ab\alpha+bc\beta+ac\alpha\beta)+ca\gamma+ab\beta\gamma+bc\alpha\gamma+(a^2+b^2+c^2)\alpha\beta\gamma\} \quad (6)$$

where p designates the number of monomeric units along the chain. Parameters involving the main geometry are shown in Figure 1.

In the adaptation of Benoit's model to PET, three virtual bonds and supplementary angles of 67° together with the bond lengths shown in Figure 2 were used. The results are summarized in Table 2. From these values, it can be seen that the agreement between statistical weighting methods and the simplified Benoit model is quite acceptable.

The previous results justified the application of the same technique to PEN and PEEK. However, some additional considerations were necessary before the method could be applied to these two polymers. First, PEN possesses a similar chemical structure to PET, the only difference being a naphthalene ring instead of a benzene ring in the PEN monomeric unit. Therefore, the virtual bond containing this change was recalculated for PEN.

Table 3. Unperturbed Dimensions of PET, PEN, and PEEK Assuming Virtual Bonds and Unperturbed, Freely Rotating Chains without Molecular Interactions

polymer	virtual bonds	$\langle r^2\rangle_0$ (Å)	$\langle s^2\rangle_0^{1/2}$ [a] (Å)
PET	3	20 740	58.8
PEN	3	23 490	62.6
PEEK	3	34 810	76.2

[a] $\langle s^2\rangle_0^{1/2}$ is the root mean squared radius of gyration.

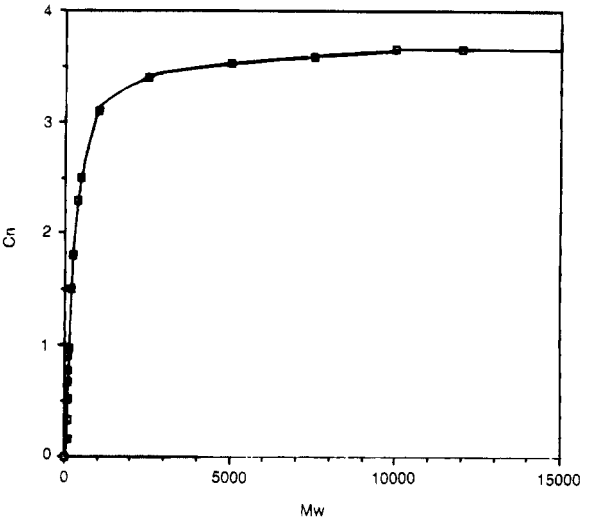

Figure 3. PEEK characteristic ratio, C_∞, after applying Benoit's model.[23]

Table 4. Lengths of Virtual Bonds, Limiting Molecular Weight, Characteristic Ratios, and Theoretical Lateral Surface Free Energies for PET, PEN, and PEEK

polymer	M_w	characteristic lengths l_1, l_2, l_3 (Å)	C_∞	σ (erg/cm^2)
PET	1×10^6	8.42, 2.97, 1.44	2.485	19.30
PEN	1×10^6	10.66, 2.97, 1.44	2.572	18.39
PEEK	1×10^6	5.50, 5.62, 5.62	3.690	12.12

In the case of PEEK, three virtual bonds and supplementary angles of 55° were used as in Bishop *et al.*[24] Table 3 shows the results for the group of polymers under consideration. Once the $\langle r^2\rangle_0$ values were obtained, the characteristic ratios were calculated using

$$C_\infty = \left.\frac{\langle r^2\rangle_0}{n\bar{l}^2}\right|_{n\to\infty} \quad (7)$$

where n is the z-number of skeletal bonds along the chain and $\bar{l}$ is the average length over the number of bonds. Since C_∞ is the characteristic ratio at infinite molecular weight, numerical calculations were made by changing the number of skeletal bonds until an asymptotic behavior was obtained for each curve. Figure 3 shows the results for PEEK. Once the characteristic ratios were obtained, calculation of the indirect values of the lateral free energies σ was completed using eq 3. A summary of results is shown in Table 4.

Experimental Section

PEEK resin was supplied by ICI-America and was grade Victrex 450fp. The gel permeation chromatography (GPC) weight-average molecular weight of this resin was 40 000. Powders were dried at 90 °C for 24 h before any experimentation. Isothermal crystallization experiments were the point

of departure in this analysis; however, the nucleation density of the as-received resin was so high that it was necessary to reprocess the polymer in boiling α-chloronaphthalene at 260 °C in order to generate films with clear nucleation patterns and measurable crystallization rates. The solvent was held at 100 °C for 5 min before increasing the temperature to 260 °C. The reflux time in solution before casting was standardized at 24 h.[25] In these experiments, samples were prepared on glass cover slips from a 0.075 wt % solution. Volumes of 0.3 mL were cast on such substrates and the samples held for 3 min at 260 °C in order to evaporate the solvent before being quenched on a cold surface. The average measured film thickness was 3 μm.

After leaving the samples in a vacuum drier for 24 h, the aforementioned preparations were melted under a nitrogen atmosphere for 2 min at 390 °C on a modified hot plate (Corning PC-351). In typical experiments, the samples were quickly transferred to a Mettler hot stage, under nitrogen, which had been preset at the crystallization temperature and was attached to an Olympus optical microscope. A sequence of micrographs was taken as a function of crystallization time at 10 °C intervals over the PEEK range of supercooling ($\Delta T \approx$ 200 °C).

PEN was kindly donated by Prof. G. Zachmann of the Institut für Technische und Makromoleculare Chemie, Universität Hamburg, FRG, and had a number-average molecular weight of 24 000. In this particular case, the nucleation density was also very high, especially at high supercoolings.[25] However, crystallization induction times and also the growth rate were lower than for PEEK, so it was decided to measure the PEN growth rate through micrography from the melt (300 °C; 3 min) without solvent reprocessing.

Determination of the lamellar thicknesses of isothermally crystallized PEEK was made through small-angle X-ray scattering (SAXS) experiments, using the 10 m system at the Oak Ridge National Laboratory, Oak Ridge, TN. This instrument[26] uses Cu Kα radiation (λ = 1.54 Å) and a 20 × 20 cm^2 position-sensitive detector with elements about 3 mm apart. It was used with a sample–detector distance of 2.74 m. The scattering intensity was stored in a 64 × 64 array. Corrections were made for instrumental background and detector efficiency (via an ^{55}Fe radioactive standard which emits γ-rays isotropically) on a cell-by-cell basis. The data were radially averaged and converted to an absolute differential cross-section by means of precalibrated secondary standards.[27] The absolute intensity is in C m^{-1} units.

Samples were crystallized using stainless-steel frames through quenching to the crystallization temperature from the melt. Experimental reproduction and sample thicknesses were optimized in order to obtain the best scattering patterns. As in the case of glass crystallized samples, crystallization experiments were made by quickly transferring the molten samples to a preset crystallization hot stage. Crystallization experiments were made from T_m = 390 °C (2 min), and the crystallization time was standardized to 1 h, after which the crystallized samples were ice-water quenched. Optimizations were also made for the position of the maximum observed in most of the SAXS experiments and also for data collection time, which was standardized to 1.25 h.

A Perkin-Elmer DSC-7 differential scanning calorimeter was used to thermally characterize portions of the isothermally crystallized PEEK. These samples were scanned from room temperature to 390 °C at 10 °C/min under nitrogen. Another set of samples was isothermally crystallized from the melt *in situ* in order to obtain the value of T_m° in accordance with the Hoffman–Weeks method.[28] The heating and cooling rates were set at 500 °C/min and the scanning rate was 10 °C/min in this latter case.

Results

Kinetics of Crystallization. One of the most important characteristics of this work was the control of the high nucleation density of the PEEK resin. This made it impossible to access the whole range of supercooling in some studies.[15,16] However, reproducible

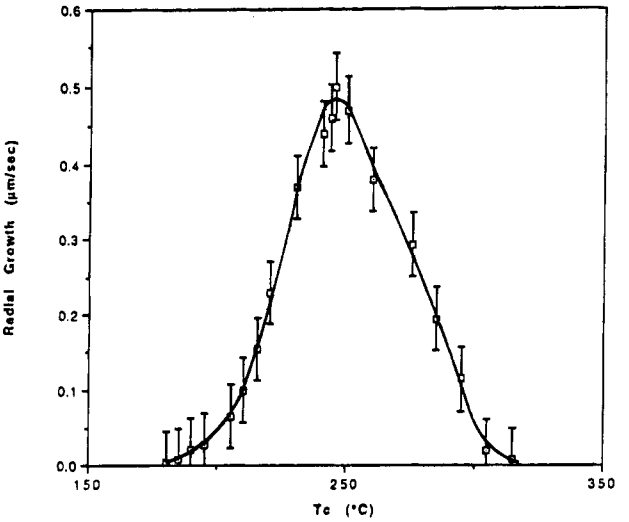

Figure 4. PEEK fastest linear growth rates. Isothermal crystallization from the melt at T_m = 380 °C; 2 min. The experimental error and best fit to the data are shown.

growth rate data in this work could be obtained under the experimental conditions described before and shown in Figure 4. It is important to mention that a variation of growth rates was observed as a function of the spherulite size and dissolution time. Spherulites nucleated at short times usually displayed a faster growth rate than those nucleating later at constant solution time before casting. On the other hand, long solution time, in general, generated high growth rates. This behavior was discussed in an earlier publication[29] and was taken as an indication of conformational changes affecting the nucleation and growth patterns of PEEK. On the basis of these studies, it was decided to use the highest crystallization rates for each crystallization temperature in what ensues.

Evaluations for PEN followed the same steps as for PEEK. However, as mentioned before, measurements were made directly from selected areas of as-received, then isothermally crystallized samples. This was because PEN developed a high nucleation density, especially at high supercoolings, and this nucleation density could not be controlled by solvent casting. Furthermore, there was a change of morphology associated with a change of crystalline structure as the degree of supercooling increased (see, for example, Buchner *et al.*[30]). Nevertheless, a well-developed bell-shaped curve representing the conjunction between nucleation and diffusion effects dominating the process of growth was determined for PEN as shown in Figure 5. The maximum in this case was located at 210 °C and crystallization conditions are such that the α crystalline form is found on the left-hand side of the crystallization curve and the β crystalline structure on the right-hand side.[30]

Experimental growth kinetics data were not obtained for PET since there is already an adequate body of data in the literature.[17,18]

SAXS data obtained were processed using conventional approaches (see later) to estimate lamellar thicknesses and hence σ_e from the dependence of lamellar thickness on inverse supercooling. A complete characterization through this approach was only applied to PEEK since reliable σ_e values already exist in the literature for PET[17,18,31] and PEN.[30] Typical corrected raw SAXS data for PEEK are shown in Figure 6.

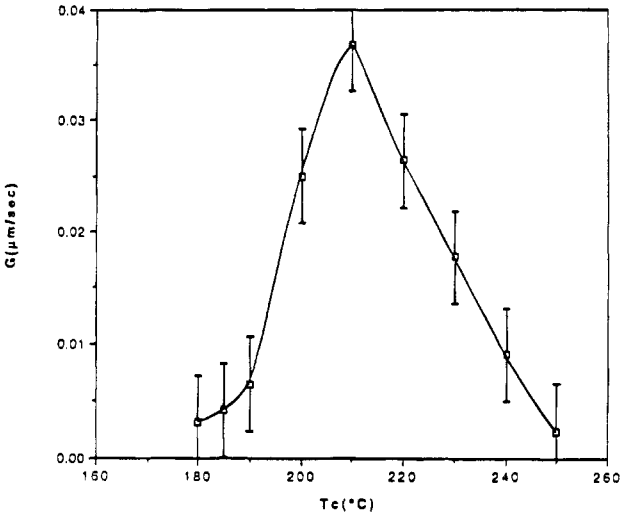

Figure 5. PEN radial growth rates. Isothermal crystallization from the melt at T_m = 300 °C; 3 min. The experimental error and best fit to the data are shown.

Discussion

Kinetics of Crystallization. A chronological mathematical sequence for the SNT model can be found in the list of references.[1-8] However, for the purposes of this work, it is enough to mention that the latest version of the model is based on three crystallization regimes as a function of the degree of supercooling. Such a crystallization process can be described by the equation

$$G = G_0 \exp[-U^*/R(T_c - T_\infty)] \exp[-K_g/T_c\Delta Tf] \quad (8)$$

where G is the radial growth rate, G_0 is an overall constant factor which depends on the molecular weight, U^* is the activation energy required to transport molecular segments to the crystallization surface, T_c is the crystallization temperature, and T_∞ is a hypothetical temperature where all movements associated with viscous flow cease. The value of T_∞ is about 51.6 °C below T_g (the glass transition temperature) for a constant "universal" value of U^* = 4120 cal/mol. ΔT is the degree of supercooling, i.e., the difference between the equilibrium melting temperature, $T_m°$, and the crystallization temperature, and f is a correction factor for the effect of temperature on the heat of fusion. The first exponential term in eq 8 takes into account the process of transport of molecular segments to the crystalline surface (transport term) and the second the incidence on the primary crystalline surface (nucleation term). The values of K_g as a function of the kind of regime of crystallization are given by

$$2K_{g_{II}} = K_{g_{III}} = 4b_0\sigma\sigma_e T_m°/(\Delta h_f)k \quad (9)$$

where $\sigma\sigma_e$ is the product of surface free energies and k is Boltzmann's constant. In accordance with eq 8, a plot of log $G + U^*/R(T_c - T_\infty)$ versus $1/T(\Delta T)f$ will show the same slopes for regimes I and III, that of regime II being half of the said value. The physical meaning of regime I is associated with a process of crystallization where the rate of lateral spreading is greater than the rate of secondary nucleation. In regime II both rates are comparable, and in regime III the rate of nucleation is expected to be much higher than that of lateral spreading. It can also be seen in eq 8 that the correlation directly generates the product of the lateral and fold surface free energies $\sigma\sigma_e$.

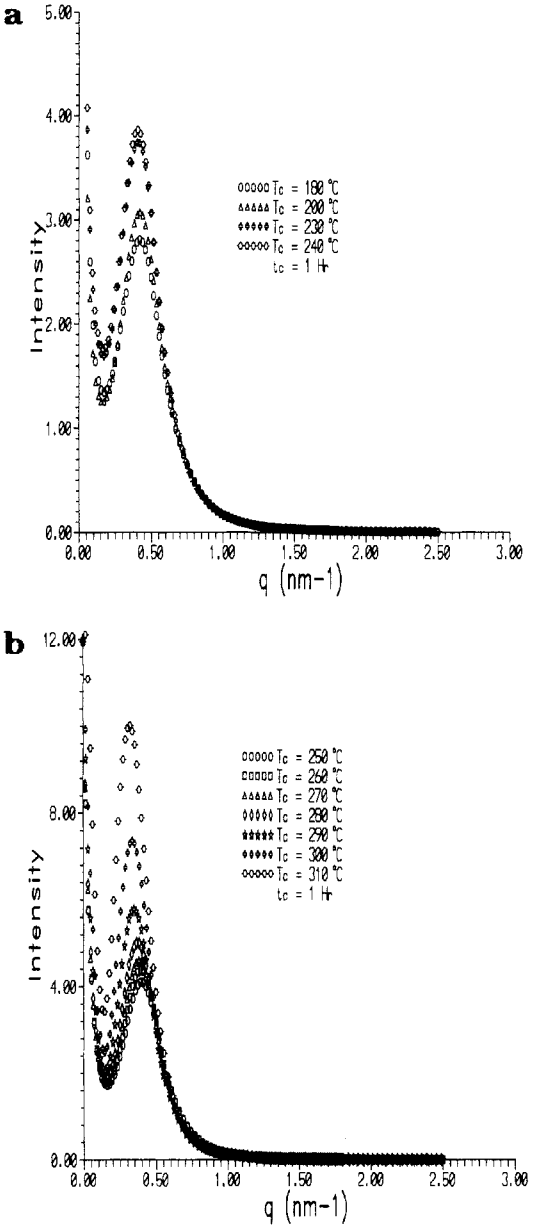

Figure 6. Raw SAXS data for isothermally crystallized PEEK (T_m = 390 °C; 2 min). The crystallization temperatures are shown.

There are two major problems in applying any secondary nucleation analysis to polymers. First, it is generally difficult to obtain experimentally the correct value of the activation energy U^* required to transport molecular segments (jump energy) to the growing crystal. The value of U^* will affect in qualitative and quantitative ways the application of the theory because a modification of this parameter can lead to changes in apparent regimes, as will be shown later. Second, there are problems in determining the equilibrium melting temperature. This hypothetical temperature will affect the correlation of the SNT model in a quantitative way without giving place to changes in regime transitions. A study of the influence of these two parameters on the procedure was therefore first conducted.

One of the most common ways of determining the value of U^* is to measure a property dependent on the segmental motion of the chains followed by the application of the Williams–Landel–Ferry (WLF)[32] equation. Because of this, a number of different values can be

found in the literature, depending on the experimental variable selected. For example, Ray–Chaudhuri[33] calculated the free volume of amorphous PEEK from the shift in the dielectric loss maximum along a logarithmic frequency axis after a change in temperature. WLF constants were obtained and a value of $U^* = 3980$ cal/mol was determined for PEEK. In this case, the fractional free volume was considered proportional to the relaxation time of the molecular segments. This approach may not be adequate because there may be other effects at the growth front which could influence the value of U^*. One such effect may be the latent heat released at the front, which may affect the U^*.

Due to the different ways of estimating the equilibrium melting temperature, $T_m°$, several values are often reported for a given polymer. One of the most common methods uses the fundamental Thomson–Gibbs equation,[34] which considers the depression of melting point that an infinitely thick crystal would suffer when it is divided into lamellar structures whose thickness is l. Another conceptual approach has been proposed by Hoffman and Weeks.[28] In this method, it is considered that the extrapolation of the experimental melting points to a line that represents a crystal that melts at its own crystallization temperature will give the equilibrium melting temperature of such crystals. It is therefore necessary to determine the melting points of isothermally crystallized samples in order to apply either of the two methods. This is usually made through DSC measurements; however, high-temperature polymers in general show multiple melting endotherms, and this often creates controversies with respect to which is the most appropriate melting point.

Blundell and Osborn,[31] for example, considered that a recrystallization phenomenon had taken place during the DSC scan of isothermally crystallized samples. Therefore, they were led to consider the melting point at the first endotherm as the one of the original isothermal crystals or the one from where extrapolations should be made in order to determine the equilibrium melting temperature. From these ideas and using the fundamental Thomson–Gibbs equation, Blundell and Osborn[31] determined a value of $T_m° = 395$ °C, and this has often been taken as the equilibrium melting temperature for PEEK. The previous concepts, however, are inconsistent with our optical microscopic observations on the melting behavior of this polymer. The results of a comprehensive study of the melting behavior will be presented in a separate publication[35] and played an important part in the choice of equilibrium melting point in this paper. In general, we have observed that PEEK is able to melt in "steps", the main melting process occurring at the higher melting endotherm. Our results using the fundamental Thomson–Gibbs equation, but melting points at the second melting endotherm, generated a $T_m° = 362$ °C. The Hoffman–Weeks approach for the second melting endotherm, on the other hand, yielded a $T_m°$ of 359 °C. These values are close to the $T_m° = 365$ °C determined by Khanna and Kumar[36] after annealing crystalline PEEK near the higher melting point. Figures 7–9 show the regime analysis for PEEK with the aforementioned $T_m°$ values and also with a range of values of U^*. The results are essentially similar to those that have been reported in the past for polymers which crystallize at high supercoolings, namely that the value of U^* is of much greater importance to the secondary nucleation analysis than that of the equilibrium melting point.

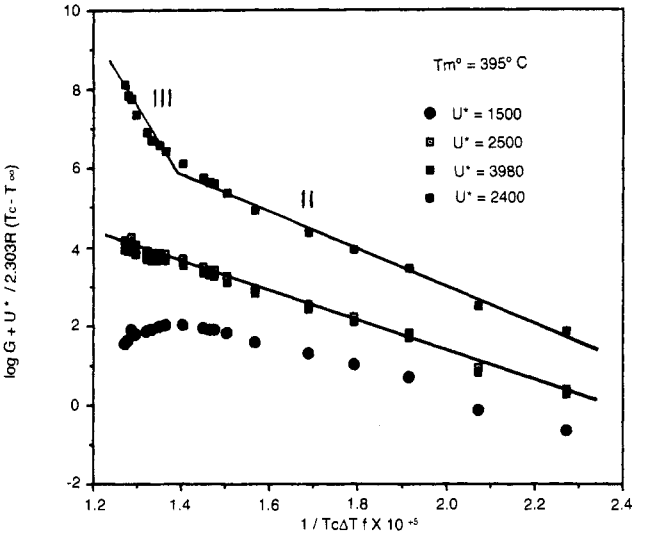

Figure 7. Regimes of PEEK with the reported $T_m° = 395$ °C and $U^* = 3980$ cal/mol together with several assumed values of U^*.

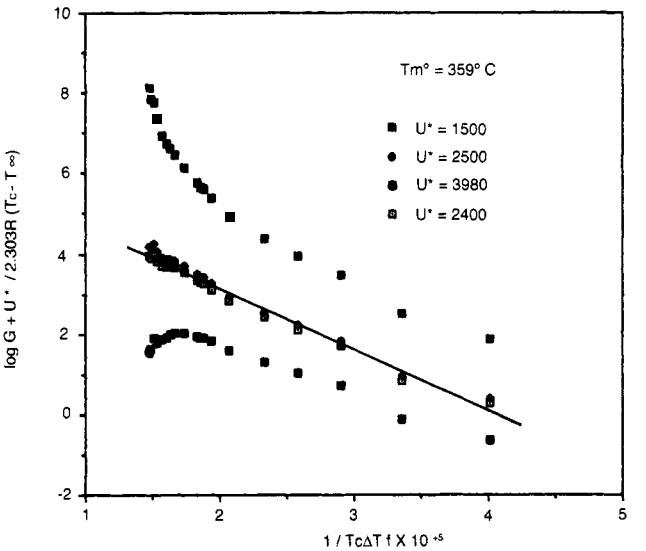

Figure 8. Regimes of PEEK using the Hoffman–Weeks $T_m°$ and several assumed values of U^*.

From these results, the critical influence of U^* in determining regime transitions is immediately observed because it affects drastically the apparent regime behavior. The reported $T_m°$ of 395 °C[29] and U^* of 3980 cal/mol[33] apparently gave a II/III regime transition. However, the ratio of the slopes is 3.7, not the expected value of 2. The same general qualitative behavior, i.e., regime transition II/III, was observed when the Thomson–Gibbs and Hoffman–Weeks $T_m°$ values were used. However, the ratio between slopes was higher: 4.65 and 4.85 for $T_m° = 362$ °C and 359 °C, respectively. Direct values of the $\sigma\sigma_\epsilon$ product for PEEK were calculated assuming regime II on the right-hand side of each plot. As explained in previous paragraphs, indirect $\sigma\sigma_e$ values were also obtained, and a summary of results for PEEK is presented in Table 5.

Regime analyses for PEN are presented in Figure 10, where a II/III regime transition appears to be present. Direct calculations for PEN are shown in Table 6. Indirect σ_e values were not obtained in this case. However, there is no reason to believe that such a value could be very high, as will be seen later with independent evaluations.

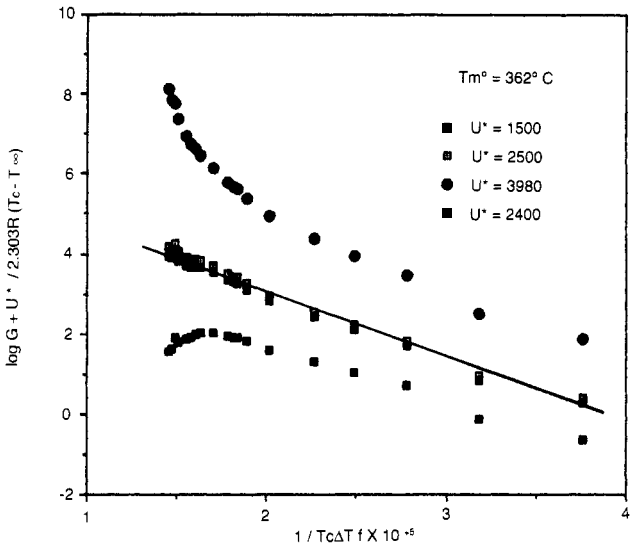

Figure 9. Regimes of PEEK using the Thomson–Gibbs $T_m°$ together with several assumed values of U^*.

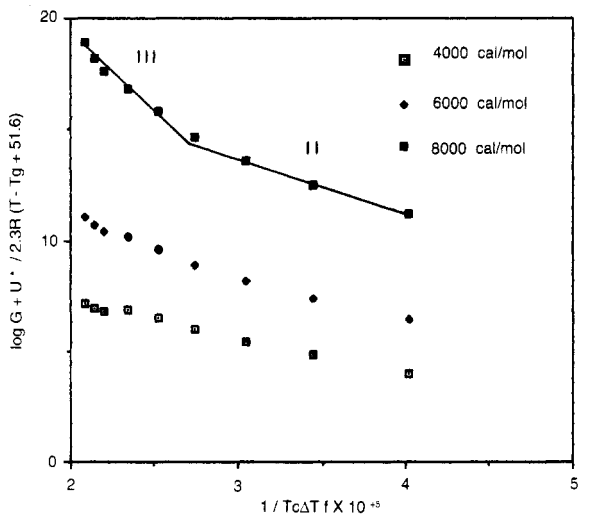

Figure 10. Regime analyses for PEN with the reported value of $T_m°$ (337 °C) and several assumed values of U^*.

Table 5. Comparison of Surface Free Energy Products of PEEK Evaluated through the Direct Application of the Secondary Nucleation Theory and Indirect Evaluations from the Same Theory

regime	U^* (cal/mol)	$T_m°$ (°C)	K_g(III)/ K_g(II)	$\sigma\sigma_{e,direct}$ (erg^2/cm^4)	σ (erg/cm^2)	σ_e (erg/cm^2)	$\sigma\sigma_{e,indirect}$ (erg^2/cm^4)
II/III	3980	359	4.85	1804			
II/III	3980	362	4.65	1979			
II/III	3980	395	3.70	4440			
		359			12.12	13.67	166
		362			12.12	14.21	172
		395			12.12	24.70	299
		359			12.12	14.74	179
		362			12.12	15.32	186
		395			12.12	25.05	304
		359			12.12	27.40	332
		362			12.12	28.90	350
		395			12.12	50.20	608

PET was studied by Palys and Phillips.[17] Crystallization in this case was made from the amorphous state. Regime II was preferred over regime I and values of $U^* = 2000$ cal/mol and $T_m° = 280$ °C were used in order to obtain the product $\sigma\sigma_e$. As shown in Table 6 the direct $\sigma\sigma_e$ products of PET are again higher than the ones obtained through indirect measurements. In a later study, Phillips and Tseng[18] studied PET again both at atmospheric and at elevated pressures. Regime III and a value of $U^* = 3050$ cal/mol were assumed in this case, which yielded again very high $\sigma\sigma_e$ products compared with the indirect calculations of the present work.

Table 6. Comparison of Surface Free Energy Products of PET and PEN Evaluated through the Direct Application of the Secondary Nucleation Theory and Indirect Evaluations for PET from the Same Theory

regime	U^* (cal/mol)	$T_m°$ (°C)	$\sigma\sigma_{e,direct}$ (erg^2/cm^4)	σ (erg/cm^2)	σ_e (erg/cm^2)	$\sigma\sigma_{e,indirect}$ (erg^2/cm^4)
			PEN			
II/III	7000	337	4898			
III	7000	337	2400			
		337		18.40		
			PET[a]			
		280		19.3	22.43	432
II	2000	280	1938			
			1942			
			1425			
			1420			
III	2000	280	969			
			971			
			712			
			710			

[a] Data taken from: Palys, L.; Phillips, P. J. *J. Polym. Sci.* **1980**, *18*, 829.

A summary of results at this point indicates a clear numerical disagreement between direct and indirect $\sigma\sigma_e$ values. However, it was necessary to consider if such a comparison was valid. The regimes version of secondary nucleation theory[2] uses a steady-state expression for the total flux of polymer from the liquid to the crystal over the nucleation barrier and relates this, on the one hand, to the lamellar thickness and, on the other hand, to the growth rate in a relatively independent way. In a similar way, the recent theoretical explanation given for the lateral surface free energy σ[8] did not emerge from a sequential mathematical derivation for the growth rate. Therefore, these alternative estimations cannot be redundant and may be taken as truly indirect evaluations.

Even though the results at this point indicate numerical disagreement, the secondary nucleation approach seems to be intuitively a good hypothesis for crystallization of semirigid macromolecules because mobility mechanisms at the growth front are prohibitively slow in crystallizing these macromolecules due to the inherent stiffness of the chain. Secondary nucleation theory considers the lamellar thickness to be a continuous function of the degree of supercooling. Alternatively, however, another approach to explain the behavior of semirigid molecules could involve a noncontinuous model. Even another option could be to use a continuous function inherent to the nature of the macromolecule rather than to the nature of the crystal *per se*.

Lamellar Thickness Estimations and σ_e. As mentioned before, indirect values of the fold surface free energy σ_e can be obtained from the kinetic expression that SNT provides[2]

$$l = 2\sigma_e T_m{}^{\circ 2}/\Delta h_f T_c \Delta T + \delta l \qquad (10)$$

where l represents the lamellar thickness. Equation 10 indicates that a plot of lamellar thickness vs the inverse of the degree of supercooling will be a straight line whose slope contains the value of σ_e.

Estimation of the lamellar thicknesses of isothermally crystallized PEEK was made through the application

of the one-dimensional correlation function of the electron density fluctuations within the sample over length ranges around 100 Å. The one-dimensional correlation function was first introduced by Vonk and Kortleve[37] in order to calculate SAXS morphology. In the present work, several corrections were applied before evaluating lamellar thicknesses. First, a four-point curvelike adjustment was applied at low values of the scattering vector $q = 4\pi \sin\theta/\lambda$, where 2θ was the scattering angle, assuming an extrapolated constant I_0 value given on average by double the intensity of the highest scattering maximum. This procedure was as consistent as other approaches such as the Debye–Bueche model given by $I(q) = A/(1 + \xi^2 q^2)$, where A is a constant and ξ is an inhomogeneity length including polynomial and lineal extrapolations. Polynomial extrapolations created uncertainties in both the shape and the $I(q)$ at $q = 0$ value and linear extrapolations affected slightly the shape of the one-dimensional correlation function. The SAXS raw data were then polynomially smoothed over the entire q range.

In a second overall adjustment of data, "background" corrections due to local electron-density fluctuations within the phases were also made. Such positive deviations from Porod's law may be related to local disorder, thermal motion, or the onset of wide-angle scattering.

On the basis of Porod's law, Ruland[38,39] suggested a method to calculate the constant background scattering intensity of SAXS data through the equation

$$I_{obs}(q)q^4 = K_P H^2(q) + I_{fl}q^4 \tag{11}$$

In accordance with eq 11 after plotting the smoothed data $I_{obs}(q)q^4$ vs q^4, the slope of the potential straight line will render the constant background scattering intensity I_{fl}, as determined in the present work with PEEK. Background-corrected data $I_{bc} = I_{obs} - I_{fl}$ were so generated after evaluation of I_{fl}.

In a third correction to the I_{bc} SAXS scattering data, a sigmoidal-gradient model for the interface was assumed in accordance with Ruland,[38] whose smoothing function is

$$H = \exp(-\sigma^2 q^2) \tag{12}$$

where σ is the standard deviation of the Gaussian smoothing function and σ^2 is the variance of the density transition. The smoothing function contains negative deviations from Porod's law which was assumed and corrected in this form at the tail of the scattering data in reciprocal space in order to determine the small-angle scattering intensities required for integrations at high q values or

$$I(q)|_{q\to\infty} = K_P \exp(-\sigma^2 q^2)/q^4 \tag{13}$$

where K_P is Porod's constant. Another form of expressing eq 9 is

$$\ln[I_{obs}q^4 - I_{fl}(q)q^4] = \ln K_P - \sigma^2 q^2 \tag{14}$$

In this form, the variance of the density transition can be determined, and this is related to the sigmoidal-gradient model interface thickness E through

$$E = (2\pi)^{1/2}\sigma \tag{15}$$

Smoothed and corrected intensities were obtained as mentioned before, and in this form, corrected data, I_{BPC}, vs q were used in order to calculate the invariant normalized, one-dimensional correlation function of the electron density fluctuations perpendicular to the main face of a stack of crystals

$$\gamma_1(r)_{BPC} = \frac{\int_0^\infty q^2 I_{BPC}(q)\cos(2\pi qr)\,dq}{\int_0^\infty q^2 I_{BPC}(q)\,dq} \tag{16}$$

A "baseline" was not observed for the range of crystallinities considered; therefore, the volume fraction crystallinity of samples was DSC evaluated[40] with the purpose of determining the "missing baseline". This was required before obtaining the average value of lamellar thickness for each experiment.[41]

Three methods were applied in order to calculate the average lamellar thickness. The first method used Bragg's law after assuming a simple two-phase model, the q value at the maximum of the Lorentz-corrected intensity, and the volume fraction crystallinity. The average lamellar thickness was calculated from $l_B = \varphi L$, where L was the average long periodicity evaluated at the maximum of the Lorentz-corrected plot.

The second method was designed by Vonk[42] assuming a linear electron density gradient across the interface whose smoothing function is a top-hat function of width E with a truncated Fourier transform[39] given by

$$H(q) = (1 - E^2 q^2/12) \tag{17}$$

A corrected Porod's law can again be used in order to obtain the interface thickness E.[40] This was obtained from the slope of the straight line expressed by

$$I_{bc}(q)q^4 = (2\pi)^4 C - (4\pi^4 C E^{2/3})q^2 \tag{18}$$

where I_{bc} is the background-corrected intensity. After determining the value of E, the number-average lamellar thickness can be calculated from the plot of the one-dimensional correlation function and

$$\langle T_c\rangle_n = OQ + \frac{E}{3}\frac{\varphi}{1-\varphi} \tag{19}$$

where OQ is the distance from $r = 0$ to the interception of the tangent of the first decay and the "baseline".[40]

In the third method, the graphical determination of the average lamellar thickness was directly obtained from the first slope of the one-dimensional correlation function and its intercept with the "baseline" at the self-correlation triangle, as suggested by Strobl and Schneider.[41]

As mentioned before, there was also an independent calculation of σ_e in this work using the fundamental Thomson–Gibbs equation

$$T_m = T_m^\circ\left(1 - \frac{2\sigma_e}{l\Delta h_f}\right) \tag{20}$$

In the case of PEEK, correlations of melting points with lamellar thicknesses were made after obtaining the corrected one-dimensional correlation function. In this form, an average value of σ_e of 22 erg/cm^2 was determined. The corresponding one-dimensional correlation functions are shown in Figure 11, and a summary of the results of lamellar thicknesses and transition layer

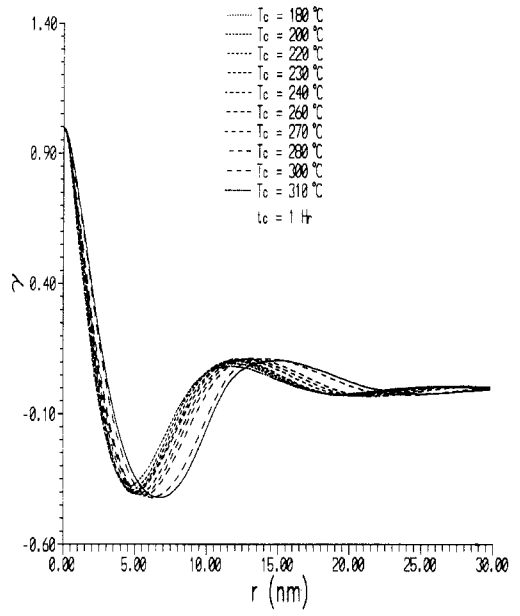

Figure 11. One-dimensional correlation functions for isothermally crystallized PEEK (T_m = 390 °C; 2 min). The crystallization temperatures are shown.

Table 7. Mass and Volume Fraction Crystallinity of PEEK Together with SAXS Morphology after Isothermal Crystallization from the Melt[a]

T_c (°C)	X_c (%)	φ	l_B (Å)	l_S (Å)	l_V (Å)	E_V (Å)	E_{RSM} (Å)
180	27.3	0.26	31.9	31.0	32.0	5.1	4.0
200	29.1	0.28	33.9	32.0	33.3	5.6	4.3
220	29.6	0.29	36.8	32.9	34.3	6.1	4.5
240	29.7	0.29	38.3	34.9	36.4	7.0	5.4
260	30.0	0.30	40.6	37.2	38.7	7.3	5.8
280	32.7	0.32	46.5	39.0	40.7	7.5	6.3
300	34.9	0.34	52.1	42.3	44.3	7.7	6.8
310	36.8	0.36	57.7	45.1	47.4	8.0	7.2

[a] B = Bragg; S = Strobl; V = Vonk; RSM = Ruland sigmoidal model.

thicknesses for PEEK emerging from the different methods is presented in Table 7.

Buchner *et al.*[30] used SAXS and Bragg's law to obtain lamellar thicknesses of PEN crystals and then used the Thomson–Gibbs method to fit the data. This rendered a value of σ_e of 60 erg/cm^2.

A value of σ_e = 93 erg/cm^2 was obtained for PET by Blundell and Osborn[31] using SAXS and the Thomson–Gibbs method. However, this value was obtained by assuming that the first melting endotherm observed in the DSC traces corresponded to isothermally generated crystals. This assumption is probably incorrect according to our observations.[35] Groeninckx *et al.*[43] determined that σ_e was a function of T_c after applying the Thomson–Gibbs equation, it being higher for lower crystallization temperatures. Nevertheless, the average reported value of σ_e was 22.3 erg/cm^2.

In studies of the effect of crystallization temperature on fold surface free energy of PET, Groeninckx *et al.*[43] showed that the value of σ_e was reduced by about 30% if the first melting endotherm was taken as the melting point rather than the second endotherm. Using the same approach, we find that a 25% reduction is found for σ_e in the case of PEEK. In the Groeninckx study these changes in value were interpreted in terms of a melting and recrystallization mechanism being responsible for the observed endotherms.

Theoretical Estimates of σ and σ_e. Calculation of the characteristic ratio C_∞ in this work permitted an estimation of the inherent stiffness of the chain through the numerical calculation of the persistence length. If wormlike chains are considered, the expression that relates the persistence length of such a model to the end-to-end distance of the unperturbed chain[44] will be given by

$$\langle r^2\rangle_0/L = 2a[1 - (a/L)(1 - e^{-L/a})] \quad (21)$$

where a is the persistence length and L is the total length of the chain. Benoit and Doty[45] evaluated higher moments of this expression and obtained the unperturbed radius of gyration as

$$\langle s^2\rangle_0/nl^2 = (\langle s^2\rangle_0/nl^2)_\infty[1 - 3(a/L) + 6(a/L) + 6(a/L)^2 - 6(a/L)^3(1 - e^{-L/a})] \quad (22)$$

Equation 22 was used to calculate persistence lengths of PEEK, PET, and PEN in this work. Another set of persistence lengths was evaluated through a simpler approach given by Flory[20]

$$(\langle r^2\rangle_0/nl^2)_\infty = 2a/l - 1 \quad (23)$$

where n is the number of skeletal bonds, l is the average length of bonds along the chain, and a is the persistence length. The results are shown in Table 8. The main characteristic of these calculations is that the persistence length increases with the inherent stiffness of the polymer chain. These results motivated us to look for a continuous or noncontinuous approach in terms of the stiffness of the molecule in this work but without success.

Table 8. Persistence Lengths of PEEK, PEN, and PET

polymer	a, Benoit's (Å)	a, Flory's (Å)
PEEK	11.81	13.03
PEN	7.85	8.96
PET	6.44	7.45

It was not possible to determine the indirect value of σ_e for PEN. However, and in order to complement and compare the results, non-model-dependent ("independent") evaluations of σ and σ_e were also made.

In the past, the most common way of evaluating the here-called "independent" lateral surface free energy was the application of the Thomas and Stavely[46] empirical approach. The method proved to be successful in the case of PE,[2] the basic Thomas and Stavely equation being expressed as

$$\sigma = \alpha\Delta H_f(a_0b_0)^{1/2} \quad (24)$$

The parameter α ranges between 0.11 and 0.30 for hydrocarbons and most of the organics, respectively. a_0 and b_0 are the molecular width and monomolecular layer thickness, respectively. The results for PEEK, PET, and PEN after applying eq 24 are shown in Table 9.

In evaluating σ, another empirical approach can also be used, consisting of the experimental determination of the surface free energy using a series of substrate materials. Such studies can be carried out using the method of Kaelble and Cirlin,[47] who found an increasing proportional relationship between crystallinity content and surface free energy for PET. Surface free energies ranged between 40 and 50 erg/cm^2 for crystallinities between 40 and 60%, respectively. It is generally known that the lamellar thickness of semicrystalline polymers

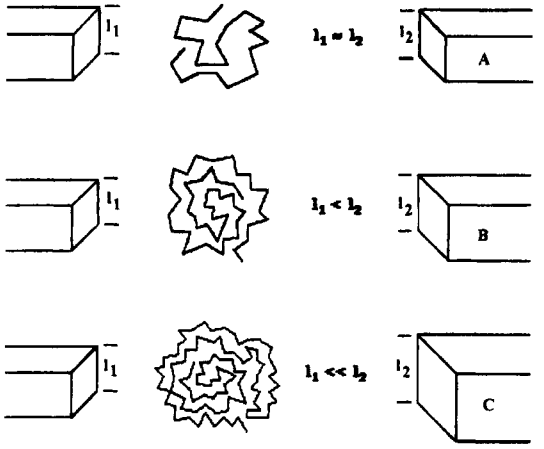

Figure 12. Flexibility on crystallization of macromolecules.

Table 9. Independent Lateral Free Energies of PEEK, PEN, and PET Obtained through the Thomas and Stavely Method[46]

polymer	α	a_0, b_0 (Å)	σ (erg/cm^2)
PEEK	0.1	4.86, 4.67	8.67
	0.3		26.01
PEN(α)	0.1	6.51, 5.66	8.82
	0.3		26.50
PET	0.1	4.56, 5.53	9.49
	0.3		28.47

increases with the crystallization temperature. So if it is assumed that at constant nucleation density an increase of crystallinity is due to the thickening of the lamellar structures, then it would be expected that a higher exposure of lamellar edges on the surface would be present in higher crystallinity films. This is likely to be the case, particularly with polymers such as PEEK and PET in which lamellar structures standing on-edge have been observed by Palys and Phillips in PET[15] and by Lovinger and Davis in PEEK.[48] It is important to note that the experimental value of σ for PET obtained through the method of Kaelble and Cirlin[47] is about double the value predicted by the "negentropic" approach (see Table 1). Therefore, and as a rough approach, the predicted values for PEEK and PEN have been doubled as shown in Table 9.

Comparison of Theoretical and Experimental Data. At this point, it can be hypothesized that there is a possible relationship between the inherent stiffness of the macromolecules and the lamellar thickness of the crystals. We need to invoke also the well-known results for polyethylene (PE).[2] The basic experimental fact is that stiffer molecules develop smaller values of lamellar thickness. If the calculated values of persistence length and the experimental lamellar thicknesses are considered, then it is seen that a smaller number of persistence lengths are involved in the crystallization process of stiff molecules than of flexible molecules. Consider for instance the attachment of coils of equivalent sizes but different intrinsic stiffness impinging on a primary nucleus of the same and constant dimensions at constant temperature in each case. If the limited experimentally observed dimensions of each type of crystal are to be finally attained, especially at high temperatures (see Figure 12), then motion along the primary nucleus must occur. The process would be very similar to the requirements of the low-Ψ form of SNT, which demands freedom at the substrate so that crystallographic register finally takes place. Stiff molecules do not have enough flexibility to meet such requirements; therefore it can be hypothesized that most of the coil instead of

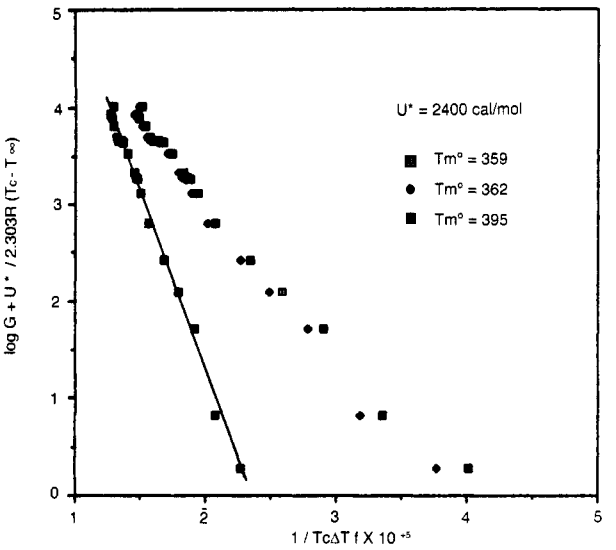

Figure 13. Single-regime behavior for PEEK and different values of $T_m°$.

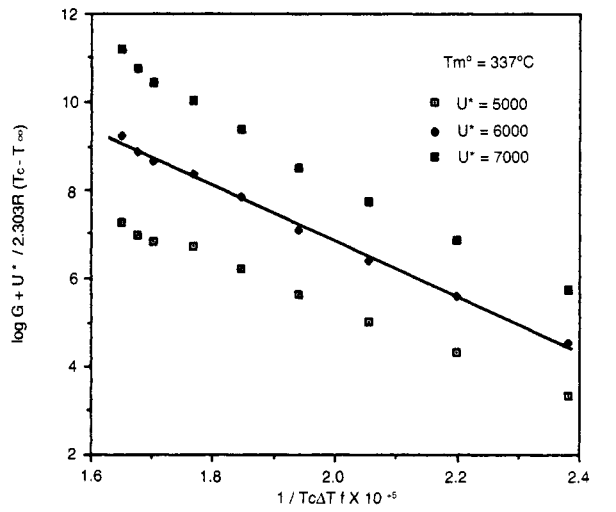

Figure 14. Single-regime behavior for PEN.

migrating on the surface in an adsorbed state is located in the amorphous phase and becomes involved in some kind of secondary crystallization. One option could be the development of secondary structures in the middle of two mother crystals,[49,50] and another the lateral rejection of crystallizable portions along the edges of primary lamellar structures which would then create lateral branching.[35]

The most obvious morphology in the previous circumstances would be one in which the unperturbed coils directly impinge on a primary nucleus where because of the intrinsic stiffness of the molecules, they are unable to easily fold back in an adjacent manner. This means that surface spreading will be the sole province of adjacent sections of other molecules. The contiguous sections of the molecule that formed the critical nucleus, if adsorbed on the surface, will be constrained to form nonadjacent folds and will function as critical nuclei themselves. In other words, an adsorbed molecule no longer forms just one critical nucleus but forms several in relatively close proximity to one another, i.e., regime III. In one attempt to test this hypothesis, regime III correlations were made as shown in Figures 13 and 14. Better numerical agreement between direct and indirect $\sigma\sigma_e$ values was obtained, as shown in Tables 6 and 10 (see also Table 5).

Table 10. Surface Free Energy Products and Kind of Regime for PEEK

regimes	U^* (cal/mol)	$T_m°$ (°C)	$\sigma\sigma_e$ (erg^2/cm^4)
II/III	3980	359	1804
II/III	3980	362	1979
II/III	3980	395	4440
III	2400	359	746
III	2400	362	811
III	2400	395	1713

Table 11. Results from Independent Evaluations of the Product of Surface Free Energies of PEEK, PEN, and PET[a]

polymer	σ_{TS} (erg/cm^2)	σ_{eTH} (erg/cm^2)	$\sigma_{TS}\sigma_{eTH}$ (erg^2/cm^4)	σ_{ST} (erg/cm^2)	$\sigma_{ST}\sigma_{eTH}$ (erg/cm^2)
PEEK	8.67	15 (B)	130	24	360
		22 [γ_1 (S)]	191		528
		25 [γ_1 (V)]	217		600
	26.01	15 (B)	316		
		22 [γ_1(S)]	572		
		25 [γ_1 (V)]	650		
PEN	8.82	60[b]	529	37	2220
	26.40		1584		
PET	9.49	25.3[c]	247	45[d]	1136
	28.47		718		

[a] TS = Thomas/Stavely; ST = surface tension; TH = thermodynamic; B = Bragg; S = Strobl; V = Vonk. [b] Source: Buchner, S.; Wiswe, D.; Zachmann, H. G. *Polymer* **1989**, *30*, 480. [c] Average value; source: Groeninckx, G.; Reynaers, H.; Berghmans, H.; Smets, G. *J. Polym. Sci., Polym. Phys. Ed.* **1980**, *18*, 1311. [d] Source: Kaelble, D. H.; Cirlin, E. H. *J. Polym. Sci., Part A-2* **1971**, *9*, 363.

As mentioned earlier, in studies of PET using the first melting endotherm with the Thomson–Gibbs equation Groeninckx et al.[43] found a reduction of σ_e of 30%. It was also mentioned that a 25% reduction was found for PEEK by ourselves using their approach. If these values of σ_e are used, it is found that the discrepancies between calculated and experimental values are even greater than presented in the tables. This point is an important one, since the work of Groeninckx *et al.*[43] for PET suggested that the values of fold energy obtained using the two different endotherms were directly related to a change in the ease of folding with temperature, higher temperatures resulting in easier folding. Although we would not dispute the general validity of their arguments, it has to be recognized that the melting behavior is influenced most by the sections of molecule which crystallize by surface spreading, since they are generally in the majority. Folding may not be present in significant amounts in the polymers being studied because of their rigidity. PET is the most flexible of the three and most likely to have folds present. However, we find the discrepancies to be present for all three polymers and so must question whether or not arguments involving chain folding rather than other forms of reentry, such as tie-molecule formation, should be considered in formulating explanations in molecular terms for any of these polymers. In the case of linear growth kinetics, we are really studying the ease of formation of the critical nucleus which may not contain any folds at all in any of the polymers being considered and so the influence of potential fold structures may be moot.

A summary of results for PEEK PET and PEN is shown in Table 11. Once again, a general disagreement can be seen between the direct application of the regimes version of SNT and independent calculations since the surface free energy products are again lower than direct model evaluations. It is important to mention that a better agreement between the model and independent calculations was observed again in all cases when regime III was adopted.

Conclusions

The crystallization behavior of semirigid macromolecules such as PEEK, PET, and PEN is characterized by high nucleation densities (especially of PEEK and PEN), changes in morphology as a function of the degree of supercooling, and local variations of growth rates of spherulites. As the rigidity of the chain increases, the growth rate and nucleation density increase. The crystallization induction time of PEN was higher than that of PET and the one of PEEK lower.

Experimental and reported values of the products $\sigma\sigma_e$ were compared through three different paths. The direct application of regime theory yielded very high values of these products in all three cases. Indirect calculations through mathematical expressions from the same theory did not agree with the ones obtained through direct correlations, the main characteristic being much lower surface free energy products. Independent free energy products were also much lower than the ones emerging from the direct application of SNT.

A strong numerical and qualitative sensitivity of secondary nucleation analyses was observed with respect to the U^* parameter. A numerical effect was also found for the equilibrium melting temperature $T_m°$.

On the basis of our experimental results, it has been determined that the regimes version of SNT does not numerically correlate with the crystallization behavior of this group of semirigid macromolecules. However, the approach was considered phenomenologicaly feasible and numerically closer to the experimental results when only regime III was assumed to exist in these polymers.

Acknowledgment. This research was supported by the Polymers Program of the National Science Foundation under Grants DMR-8719028 and DMR-9107675 and, in part, by the Division of Materials Sciences, U.S. Department of Energy, under Contract No. DE-AC05-84OR21400.

References and Notes

(1) Hoffman, J. D.; Weeks, J. J. *J. Chem. Phys.* **1962**, *36*, 1723.
(2) Hoffman, J. D.; Davies, G. T.; Lauritzen, J. I., Jr. *Treatise in Solid State Chemistry*; Hannay, N. B., Ed.; Plenum Press: New York, 1976; Chapter 7.
(3) Hoffman, J. D. *Polymer* **1983**, *24*, 3.
(4) Hoffman, J. D. *Polymer* **1985**, *25*, 1763.
(5) Hoffman, J. D.; Miller, R. L. *Macromolecules* **1988**, *21*, 3038.
(6) Hoffman, J. D. *SPE ANTEC Proc.* **1989**, 288.
(7) Hoffman, J. D. *Polymer* **1992**, *33*, 2643.
(8) Hoffman, J. D.; Miller, R. L.; Marand, H.; Roitman, D. B. *Macromolecules* **1992**, *25*, 2221.
(9) Sadler, D. M.; Gilmer, G. H. *Polymer* **1984**, *25*, 1446.
(10) Sadler, D. M. *Polym. Commun.* **1986**, *27*, 143.
(11) Sadler, D. M. *J. Chem. Phys.* **1987**, *87*, 1771.
(12) Sadler, D. M. *Polymer* **1987**, *28*, 1440.
(13) Phillips, P. J. *Rep. Prog. Phys.* **1990**, *53*, 549.
(14) Phillips, P. J. *Handbook of Crystal Growth*; Hurle, D. T. J., Ed.; Elsevier: New York, 1994; Vol. 2.
(15) Day, M.; Deslandes, Y.; Roovers, J.; Suprunchuk, T. *Polymer* **1991**, *32*, 1258.
(16) Deslandes, Y.; Sabir, F.-N.; Roovers, J. *Polymer* **1991**, *32*, 1267.
(17) Palys, L. H.; Phillips, P. J. *J. Polym. Sci., Polym. Phys. Ed.* **1980**, *18*, 829.
(18) Phillips, P. J.; Tseng, H. T. *Macromolecules* **1989**, *22*, 1649.
(19) Billmeyer, F. W., Jr. *Textbook of Polymer Science*; Wiley: New York, 1984.

(20) Flory, P. J. *Statistical Mechanics of Chain Molecules*; Wiley: New York, 1969.
(21) Boyd, R. H.; Phillips, P. J. *The Science of Polymer Molecules*; Cambridge University Press: Cambridge, 1993.
(22) Williams, A. D.; Flory, P. J. *J. Polym. Sci., Part A-2* **1967**, *5*, 417.
(23) Benoit, H. *J. Polym. Sci.* **1948**, *3*, 376.
(24) Bishop, M. T.; Karasz, F. E.; Russo, P. S.; Langley, K. H. *Macromolecules* **1985**, *18*, 86.
(25) Medellín-Rodríguez, F. J. Ph.D. Dissertation, University of Tennessee, 1993.
(26) Wignall, G. D.; Lin, J. S.; Spooner, S. *J. Appl. Crystallogr.* **1990**, *23*, 241.
(27) Russell, T. P.; Lin, J. S.; Spooner, S.; Wignall, G. D. *J. Appl. Crystallogr.* **1988**, *21*, 629.
(28) Hoffman, J. D.; Weeks, J. J. *J. Chem. Phys.* **1962**, *37*, 1723.
(29) Medellín-Rodriguez, F. J.; Phillips, P. J. *Polym. Eng. Sci.*, accepted.
(30) Buchner, S.; Wiswe, D.; Zachmann, H. G. *Polymer* **1989**, *30*, 480.
(31) Blundell, D. J.; Osborn, B. N. *Polymer* **1983**, *24*, 953.
(32) Ferry, J. D. *Viscoelastic Properties of Polymers*; Wiley: New York, 1980.
(33) Ray-Chaudhuri, T. Ph.D. Dissertation, University of Tennessee, 1993.
(34) Bassett, D. C. *Principles of Polymer Morphology*; Cambridge University Press: Cambridge, 1981.
(35) Medellín-Rodríguez, F. J.; Phillips, P. J., unpublished data, 1994.
(36) Khanna, Y. P.; Kumar, R. *J. Polym. Sci., B: Polym. Phys. Ed.* **1989**, *26*, 369.
(37) Vonk, C. G.; Kortleve, G. *Kolloid-Z.* **1967**, *220*, 19.
(38) Ruland, W. *J. Appl. Crystallogr.* **1971**, *4*, 70.
(39) Koberstein, J. T.; Morra, B.; Stein, R. S. *J. Appl. Crystallogr.* **1980**, *13*, 34.
(40) Defoor, F. Ph.D. Dissertation, Katholieke Universiteit te Leuven, 1992.
(41) Strobl, G. R.; Schneider, M. *J. Polym. Sci., Polym. Phys. Ed.* **1980**, *18*, 1343.
(42) Vonk, C. G. *J. Appl. Crystallogr.* **1973**, *6*, 81.
(43) Groeninckx, G.; Raynaers, H.; Berghmans, H.; Smets, G. *J. Polym. Sci., Polym. Phys. Ed.* **1980**, *18*, 131.
(44) Kratky, O.; Porod, G. *Recl. Trav. Chim. Pays-Bos* **1949**, *68*, 1106.
(45) Benoit, H.; Doty, P. *J. Phys. Chem.* **1953**, *57*, 958.
(46) Thomas, D. G.; Stavely, L. A. K. *J. Chem. Soc.* **1952**, 4569.
(47) Kaelble, D. H.; Cirlin, E. H. *J. Polym. Sci., Part A-2* **1971**, *9*, 363.
(48) Lovinger, A. J.; Davis, D. D. *Polym. Commun.* **1985**, *26*, 322.
(49) Bassett, D. C.; Olley, R. H.; Al Raheil, I. A. M. *Polymer* **1988**, *29*, 1745.
(50) Hsiao, B. S.; Gardner, K. H.; Wu, D. Q. *Polymer* **1993**, *34*, 3996.

MA9500852